Supporting Information

Investigation of High Oxygen Reduction Reaction Catalytic Performance on Mn-based Mullite $SmMn_2O_5$

Jieyu Liu,[a,†] Meng Yu,[a,†] Xuewei Wang,[b] Jie Wu,[c] Changhong Wang,[d] Lijun Zheng,[a] Dachi Yang,[a] Hui Liu,[a] Yan Yao,[e] Feng Lu,[a*] and Weichao Wang[a,f*]

[a]College of Electronic Information and Optical Engineering, Nankai University, Tianjin 300350, China

[b]School of Materials Science and Engineering, Tianjin University of Technology, Tianjin 300384, China

[c]College of Material Science and Engineering, Shandong University of Science and Technology, Qingdao 266590, China

[d]School of Science, Tianjin University of Technology, Tianjin 300384, China

[e]Department of Electrical and Computer Engineering and Materials Science and Engineering Program, University of Houston, Houston, TX 77204, USA

[f]Department of Materials Science and Engineering, University of Texas at Dallas, Richardson, TX 75080, USA

[†]These authors contributed equally to this work.

*Corresponding authors: weichaowang@nankai.edu.cn, lufeng@nankai.edu.cn

S1. Bulk $SmMn_2O_5$ mullite phase diagram deduction

Following the computational hydrogen electrode (CHE) method proposed by Norskov,[1-3] zero voltage is defined based on the reversible hydrogen electrode (RHE), in which the reaction

$$H^+ + e^- \rightarrow {}^1/_2 H_2 \quad (1)$$

is defined to be in equilibrium at zero voltage, at all values of pH, at all temperatures, and with H_2 gas pressure at 101325 Pa.

Thus, the total chemical potential of the proton-electron pair as a function of applied potential U can be calculated as:

$$\mu_{H^+} + \mu_{e^-}(U) = {}^1/_2 \mu_{H2} - eU \quad (2)$$

The oxygen chemical potential then can be interpreted as:

$$\mu_O(U, pH) = \mu_{H_2O} - 2\left(\mu_{H^+} + \mu_{e^-}(U)\right) = \mu_{H_2O} - \mu_{H2} + 2eU \quad (3)$$

0.1 M KOH was used as the electrolyte for oxygen reduction reaction (ORR) activity characterization in our experiment, for simplicity, the corresponding pH in this work is referred to the experimental condition, i.e. pH = 13

The chemical potential of each element in $SmMn_2O_5$ crystal is related by the Gibbs free energy of the bulk oxide:[4]

$$\mu_{Sm}^{SmMn_2O_5} + 2\mu_{Mn}^{SmMn_2O_5} + 5\mu_O(U, pH = 13) = E_{SmMn_2O_5}^{bulk} \quad (4)$$

$\mu_{Sm}^{SmMn_2O_5}$, $\mu_{Mn}^{SmMn_2O_5}$ and $\mu_O(U, pH = 13)$ are the chemical potentials of samarium, manganese and oxygen, respectively. $E_{SmMn_2O_5}^{bulk}$ is the total energy of bulk per formula unit $SmMn_2O_5$.

Take $\mu_{Mn}^{SmMn_2O_5}$ as the independent chemical potential.

Rearranging equation (4):

$$\mu_{Mn}^{SmMn_2O_5} = {}^{1}/_{2}[E_{SmMn_2O_5}^{bulk} - \mu_{Sm}^{SmMn_2O_5} - 5\mu_O(U,\ pH = 13)] \quad (5)$$

For binary metal oxides, the chemical potential of metals can be written as:

$$\mu_{M}^{MO_n} = E_{DFT}^{MO_n} - n\mu_O(U,\ pH = 13) \quad (6)$$

where M denotes the metal element (Sm or Mn), and $E_{DFT}^{MO_n}$ is the calculated total energy of the corresponding oxides. To prevent bulk $SmMn_2O_5$ from decomposing into lower order binary metal oxides, the chemical potential of a metal constituent in the mullite should be smaller than that in the lower order binary metal oxides:

$$\mu_{M}^{SmMn_2O_5} < \mu_{M}^{MO_n} \quad (7)$$

We then use the chemical potential deviation of samarium from the elementary crystal to construct the phase diagram.

$$\Delta\mu_{Sm} = \mu_{Sm} - E_{Sm}^{bulk} \quad (8)$$

S2. Passivation of 8-layer (001) MnO_3-2 slab

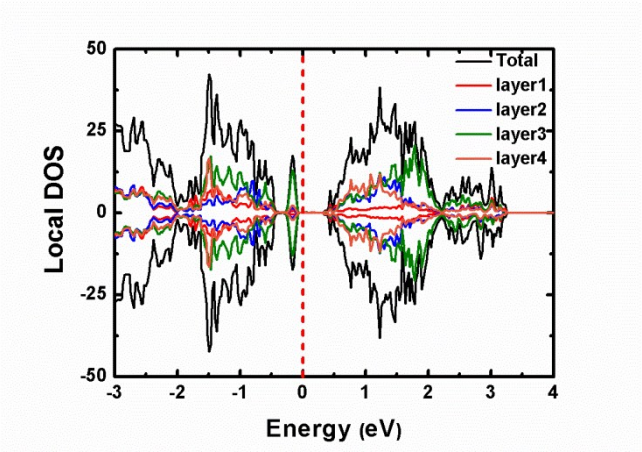

Figure S1. The local density of states (LDOS) of layer-1 to layer-4 of the 8-layer (001) MnO_3-2 slab. The black line represents the total DOS of the bottom four layers (layer-1 to layer-4).

S3. Stability of mullite $SmMn_2O_5$ (001) surfaces

The relative stability of $SmMn_2O_5$ (001) surfaces under the given applied potential (U = 0.8 V) and pH (pH = 13) were calculated based on the following equation:[4]

$$\Gamma_i = \frac{1}{A_s}[E_{total}^{\ i} - N_O\mu_O(U = 0.8\,V, pH = 13) - N_{Mn}\mu_{Mn}^{SmMn_2O_5} - N_{Sm}\mu_{Sm}^{SmMn_2O_5}] \quad (9)$$

where Γ_i is the surface energy, i donates the type of slab, A_s is the surface area of the (2×1) (001) slab, $E_{total}^{\ i}$ is the calculated total energy of the slab. N_o, N_{Mn} and N_{Sm} are the numbers of O, Mn and Sm atoms in the slab, respectively. $\mu_O(U = 0.8\,V, pH = 13)$ is defined as equation (3). $\mu_{Mn}^{SmMn_2O_5}$ is the chosen independent chemical potential, which is connected with $\mu_{Sm}^{SmMn_2O_5}$ by equation (5).

S4. Linear relations of binding energies

The calculated binding energies of O* (ΔE_{O^*}), OH* (ΔE_{OH^*}), OO* (ΔE_{OO^*}) and OOH* (ΔE_{OOH^*}) are defined as the reaction energies of the following reactions:

$$H_2O^{(g)} + * \rightarrow O^* + H_2^{(g)} \quad (10)$$

$$H_2O^{(g)} + * \rightarrow OH^* + {}^1/_2 H_2^{(g)} \quad (11)$$

$$2H_2O^{(g)} + * \rightarrow OO^* + 2H_2^{(g)} \quad (12)$$

$$2H_2O^{(g)} + * \rightarrow OOH^* + {}^3/_2 H_2^{(g)} \quad (13)$$

where * donates an adsorption site on the surface. H_2O and H_2 are in the gas phase. Thus:

$$\Delta E_{O^*} = E_{DFT}^{O^*} + E_{H_2(g)} - E_{H_2O(g)} - E_* \quad (14)$$

$$\Delta E_{OH^*} = E_{DFT}^{OH^*} + {}^1/_2 E_{H_2(g)} - E_{H_2O(g)} - E_* \quad (15)$$

$$\Delta E_{OO^*} = E_{DFT}^{OO^*} + 2E_{H_2(g)} - 2E_{H_2O(g)} - E_* \quad (16)$$

$$\Delta E_{OOH^*} = E_{DFT}^{OOH^*} + {}^3/_2 E_{H_2(g)} - 2E_{H_2O(g)} - E_* \quad (17)$$

S5. Theoretical activity

The free energy change for each step in the main test can be calculated as:[1-3]

$$\Delta G_i = \Delta E_i + \Delta(ZPE)_i - T\Delta S_i + eU + \kappa T In10 \times \Delta pH \quad (18)$$

where i = 1, 2, 3, 4 corresponds to steps from Equation (1) to (4) in the main test, ΔE is the reaction energy, ΔZPE is the change of zero-point energy, T is temperature, ΔS is the difference in entropy, U is the electrode potential vs. standard hydrogen electrode (SHE) and κ is boltzmann constant. All these parameters can be obtained from DFT calculations or standard tables for gas-phase molecules.[5]

At any pH, the following half-reaction:

$$H_2O_{(l)} + e^- \leftrightarrow OH^-_{(aq)} + {}^1\!/_2 H^{(g)}_2 \quad (19)$$

has a potential of 0 V vs. RHE.[6] At this potential, the reaction is at equilibrium, and thus chemical potentials can be written as Equation (20) at any U:

$$\mu_{H_2O_{(l)}} + \mu_{e^-}(U) = {}^1\!/_2\mu_{H_2(g)} + \mu_{OH^-_{(aq)}} - eU \quad (20)$$

Rearranging Equation (20), the chemical potential difference between OH^- and e^- can be found to be:

$$\mu_{OH^-_{(aq)}} - \mu_{e^-}(U) = \mu_{H_2O_{(l)}} - {}^1\!/_2\mu_{H_2(g)} + eU \quad (21)$$

The first step of the four-electron pathway is the displacement of OH* by OO*.

$$\Delta G_1 = G_{OO^*} + [\mu_{OH^-_{(aq)}} - \mu_{e^-}(U)] - G_{OH^*} - G_{O_2} \quad (22)$$

where G_{OO*} and G_{OH*} are the free energies of the surface slab with OO* and OH* adsorption repectively and could be written in terms of DFT energies:

$$G_{OO^*} = E^{OO^*}_{DFT} + ZPE_{OO^*} - TS^{0}_{OO^*} \quad (23)$$

$$G_{OH^*} = E_{DFT}^{OH^*} + ZPE_{OH^*} - TS_{OH^*}^{0} \quad (24)$$

Combine Equation (15) and (16), we get the relationship:

$$E_{DFT}^{OO^*} - E_{DFT}^{OH^*} = \Delta E_{OO^*} - \Delta E_{OH^*} - {}^{3}/_{2}E_{H_2(g)} + E_{H_2O(g)} \quad (25)$$

According to the linear relationship:

$$\Delta E_{OH^*} = 0.62\Delta E_{O^*} - 0.87 \quad (26)$$

$$\Delta E_{OO^*} = 0.86\Delta E_{O^*} + 2.68 \quad (27)$$

Substitute equations (23) – (27) into (22), then:

$$\Delta G_1 = 0.24\Delta E_{O^*} - 1.61 \quad (28)$$

Similarly:

$$\Delta G_2 = -0.14\Delta E_{O^*} - 0.32 \quad (29)$$

$$\Delta G_3 = 0.28\Delta E_{O^*} - 2.47 \quad (30)$$

$$\Delta G_4 = -0.38\Delta E_{O^*} - 0.52 \quad (31)$$

S6. Two-electron pathway

We considerd a similar associative mechanism for the less efficient two-electron pathway for hydrogen peroxide production.

$$OH^* + O_2 + e^- \rightarrow OO^* + OH^- \quad (32)$$

$$OO^* + H_2O + e^- \rightarrow OOH^* + OH^- \quad (33)$$

$$OOH^* + H_2O + e^- \rightarrow H_2O_2 + OH^- \quad (34)$$

In this case, the equilibrium potential is 0.68 V.[7] We ploted the free energy evolution diagram in Figure S2. It is shown that the potential is limited by the protonation from OO^* to OOH^* on the surface of MnO_3-1 slab. The ORR steps in the two-electron pathway are thermodynamically favorable only under low electrode potential.

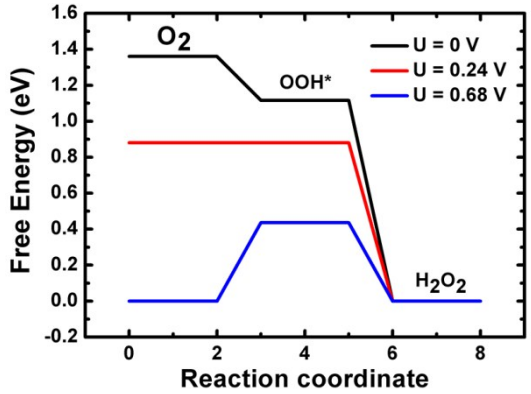

Figure S2. The free energy diagram of two-electron pathway to produce H_2O_2 on the surface of MnO_3-1 slab.

S7. Synthesis of $SmMn_2O_5$, and MnO_x

All metal salt precursors were analytical grade and used as received. 0.2777 g $Sm(NO_3)_3•6H_2O$ (Aladdin) was dissolved in 50 ml deionized water (18.25 MΩ) followed by adequate stirring. Then 0.0593 g $KMnO_4$ and 0.2143 g $Mn(CH_3COO)_2•6H_2O$ (Aladdin) were added to the solution simultaneously and constantly stirred for at least 30 min. The corresponding mole ratio of Sm-to-Mn is approximately 1:2. 5.5 mL NaOH (1 M) was dropwise added to the mixture and continued to stir for several minutes. After that, the precursor was transferred into a 100 ml stainless steel Teflon-lined autoclave, followed by a standard hydrothermal treatment at 200 ℃ for 24 h. The final precipitate was washed with nitric acid (5%) and distilled water for several times, and dried at 100 ℃ for 12 h. MnO_x was prepared via the similar procedure without adding $Sm(NO_3)_3•6H_2O$. If we change the ratio of Sm-to-Mn, final product**s** would become a mixture of $SmMn_2O_5$, MnO_x and even $Sm(OH)_3$ **(**Figure S3**)**. Specifically, extra Sm might introduce $Sm(OH)_3$**,** while excessive Mn could lead to complicated MnO_x**.**

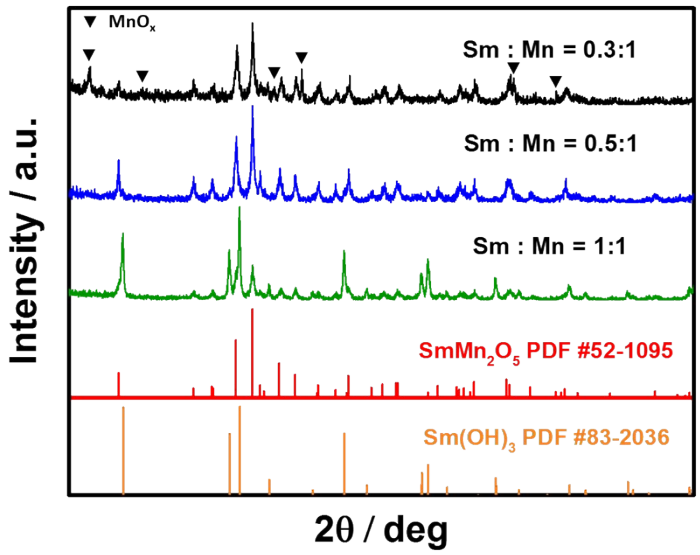

Figure S3. XRD spectra of the as-prepared $SmMn_2O_5$ and the reference samples by changing the stoichiometric ratio of metal precursors.

S8. Electrode preparation

The catalyst inks were prepared by physically mixing 5 mg of catalyst powder and/or 3 mg of Vulcan X-72 (Carbot Corp.) with 30 μL of Nafion (5 wt. %, Aldrich) and 970 μL of ethanol, followed by at least 40 min ultrasonication to form homogeneous mixtures.[8] 10 μL of these mixtures were carefully dropped onto glassy-carbon (GC) electrodes (5-mm diameter) and dried in a sealed glass beaker which had been pre-saturated with ethanol vapor in order to slow down drying rate, which was proven to be important for obtaining uniform coatings.[9, 10] Finally, all of the electrodes had a composition of 250 μg_{oxide} cm^{-2}_{disk} and/or 150 μg_{carbon} cm^{-2}_{disk}, except for Pt/C used as a reference. The Pt/C catalyst ink was made by dispersing Pt/C (Johnson Matthey

Corp.) in a water-isopropanol solution, of which 25 μg_{Pt} cm^{-2}_{disk} was applied to the electrode. Before each measurement, GC electrodes were polished with 0.3 μm and then 0.05 μm alumina slurry to maintain mirror-like surfaces.[11]

S9. Electrochemical analysis

The number of electrons transferred (n) was calculated from the slope of the best fitted lines of Koutecky–Levich plot (J^{-1} vs. $\omega^{-0.5}$) at different potentials. The Koutecky–Levich equation is given as below:

$$\frac{1}{J} = \frac{1}{J_L} + \frac{1}{J_K} = \frac{1}{B\omega^{0.5}} + \frac{1}{J_K} \quad (35)$$

$$B = 0.62nFC_{O_2}D_{O_2}^{2/3}v^{-1/6} \quad (36)$$

$$J_K = nFkC_{O_2} \quad (37)$$

where J is the measured current density, J_L and J_K are known as the diffusion-limited and kinetic-limited current density of ORR, respectively.[12] F (96485 C mol^{-1}) is the Faraday constant, C_{O_2} (1.2×10^{-6} mol cm^{-3}) is the bulk concentration of oxygen, D_{O_2} (1.9×10^{-5} cm^2 s^{-1}) is the diffusion constant for oxygen in 0.1 M KOH and v (0.01 cm^2 s^{-1}) is the kinetic viscosity.[13] The constant 0.62 in B is adopted when the rotating speed ω is expressed in rad/s. The Tafel slope was obtained from Tafel's equation:

$$\eta = a + blg\,J_K \quad (38)$$

where η represents the overpotential, and J_K is the kinetic current density with mass-transport correction by

$$J_K = \frac{J_L \times J}{J_L - J} \tag{39}$$

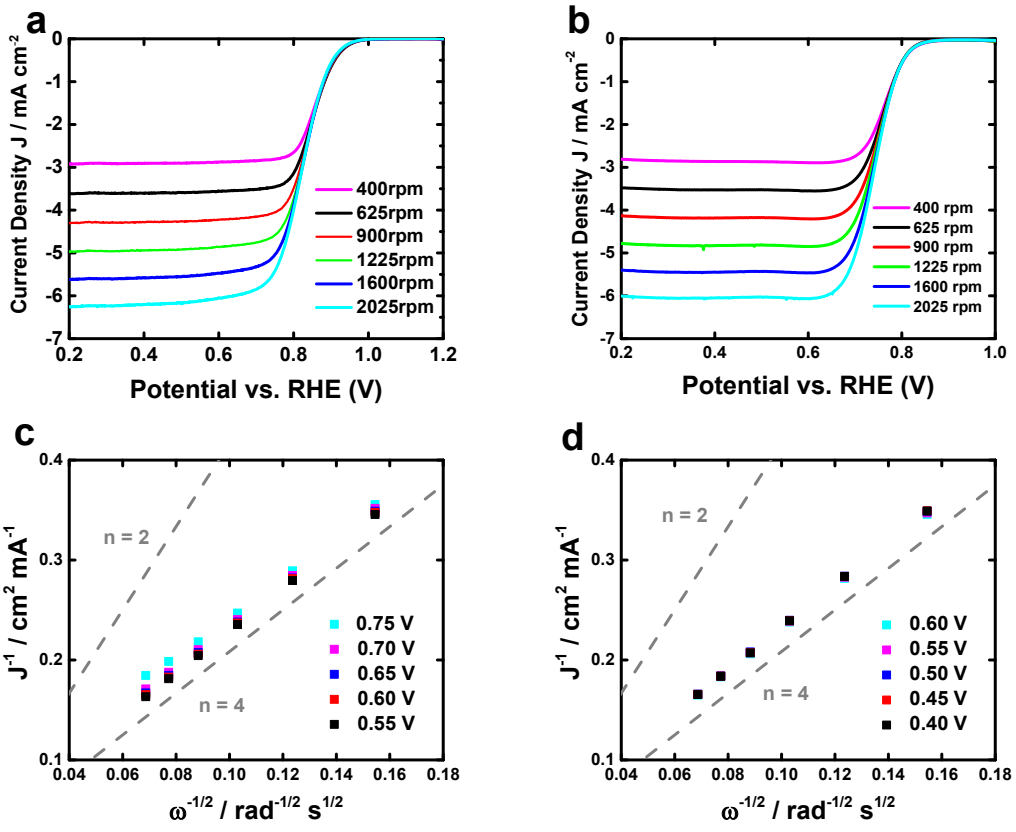

Figure S4. LSV curves of (a) Pt/C and (b) $SmMn_2O_5$-NRs/C at various rotating speed, and the corresponding K-L plots of (c) Pt/C and (d) $SmMn_2O_5$-NRs/C at different potentials.

For RRDE analysis, the electron transfer number and proportion of peroxide were calculated by

$$n = \frac{4I_D}{I_D + (I_R/N_C)} \tag{40}$$

$$\%HO_2^- = 100\frac{2(I_R/N_C)}{I_D + (I_R/N_C)} \tag{41}$$

where I_D and I_R are the disk and ring current, respectively. N_C is the calibrated collection efficiency.

The calibration process follows the one reported by previous researchers.[14] Briefly, the collection efficiency (N_C) was calibrated in Ar-saturated electrolyte with 0.1 M KOH and 4 mM $K_3Fe(CN)_6$, using the same electrodes as those used in ORR measurements. The electrodes were rotated at a certain angular velocity and then chronoamperometric measurement was performed. The disk and ring potential were fix to be 0.1 V and 1.5 V vs. RHE, respectively. The N_C is calculated according to the following equation

$$N_C = \frac{I_R - I_{R_0}}{I_D} \tag{42}$$

where I_D and I_R are the disk and ring current averaged over the last 10 s during 60 s measurements. I_{R_0} is the averaged ring current with the disk disconnected.

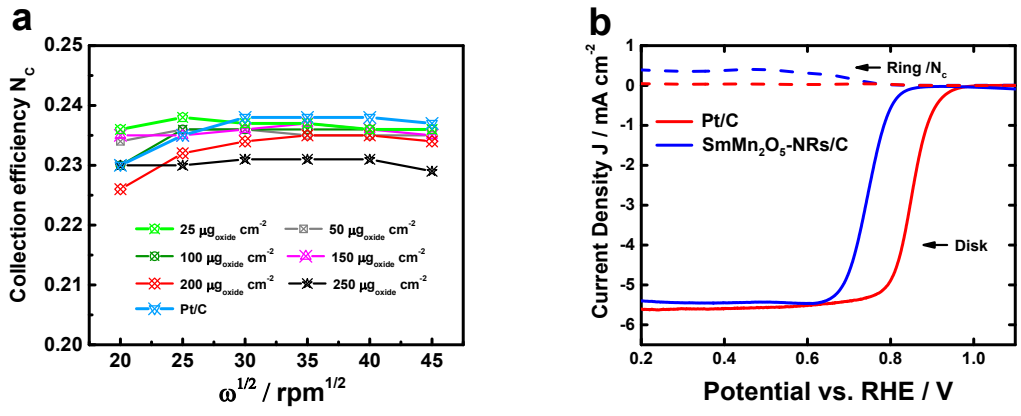

Figure S5. (a) N_C of RRDE loaded with catalysts. (b) Oxygen reduction currents at ring and disk $SmMn_2O_5$-NRs/C and Pt/C catalysts.

S10. Electrochemical impedance spectroscopy (EIS) analysis

EIS measurement of $SmMn_2O_5$ catalyst (250 μg cm^{-2}_{disk}) was performed at 0.84 V vs. RHE in 0.1 M KOH from 10 kHz to 0.1 Hz. A sinusoidal voltage with an amplitude of 10 mV was applied to the initial voltage. The ohmic resistance of electrolyte between working and reference electrode (R_s) was observed to be ~42 Ω from Figure S6. The corrected potential was calculated by the following equation:

$$E_{iR-corrected} = E_{applied} - iR_s \quad (43)$$

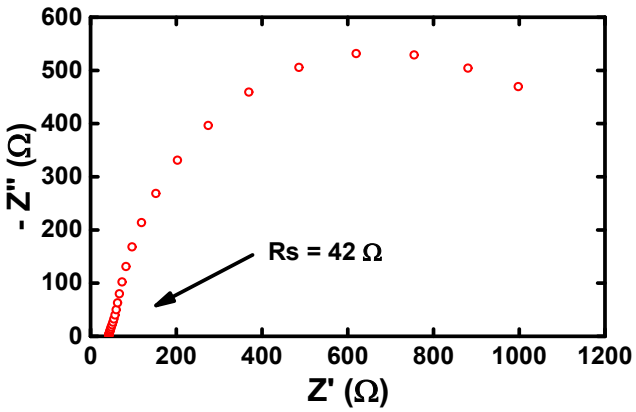

Figure S6. EIS plot of $SmMn_2O_5$ NRs .

S11. ORR acitvity comparation

Table S1. The ORR activities of selected manganese-based oxides.

Catalyst	E_{onset} (V vs. RHE)	$E_{1/2}$ (V vs. RHE)	J_L (mA/cm^2)	n	Structure	Ref.
$SmMn_2O_5$/C	0.817	0.746	5.45	3.78	Nanorod	This work
α-MnO_2/GC	0.89⊥	0.8⊥	3.4*	3.89	Nanorod	15
β-MnO_2/C	0.85	0.7	2.77	2.4	Nanorod	16
σ-MnO_2/C	0.7	0.66	2.67	2.4	Microsphere	16
MnO_x	0.83⊥	0.73	5.7	NA	Thin film	17
Mn_3O_4@NGO	0.83	0.66⊥	3.7	3.81	Ellipsoid	18
MnO@GC	0.77⊥	0.64⊥	4.5⊥	NA	Nanoparticle	19

* The diameter of GC electrode is 4 mm.

⊥ Estimated form LSV.

S12. Supporting data

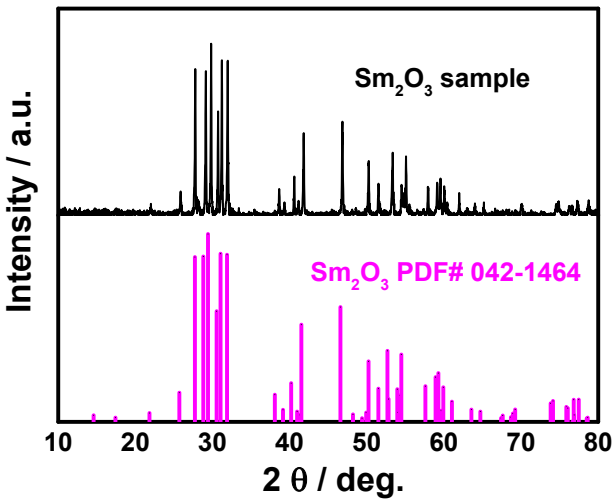

Figure S7. XRD spectra of Sm_2O_3.

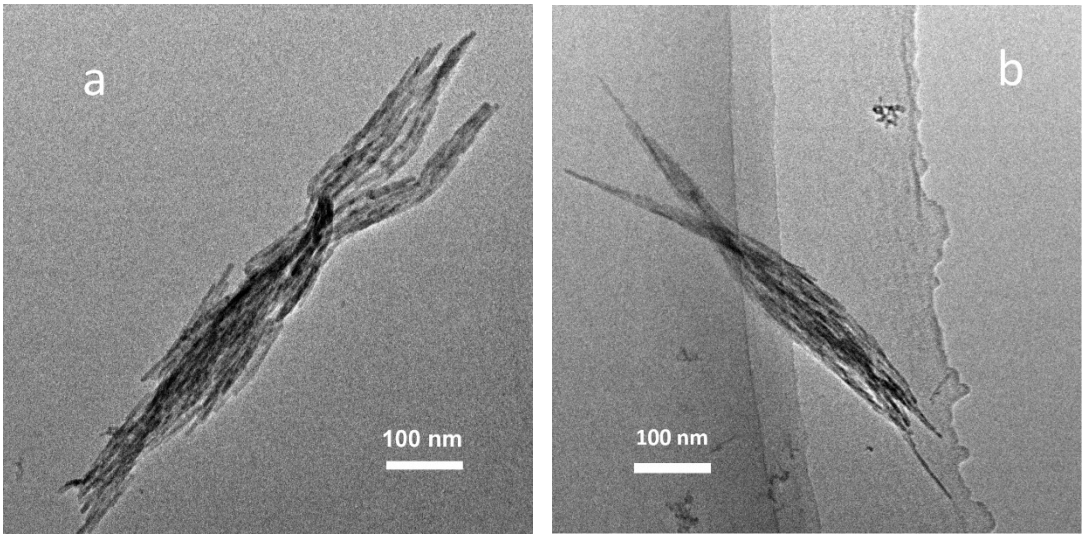

Figure S8. Representative TEM images of $SmMn_2O_5$-NRs

Reference

1. J. K. Nørskov, J. Rossmeisl, A. Logadottir, L. Lindqvist, J. R. Kitchin, T. Bligaard and H. Jónsson, *J. Phys. Chem. B*, 2004, **108**, 17886-17892.
2. J. Rossmeisl, J. K. Nørskov, C. D. Taylor, M. J. Janik and M. Neurock, *J. Phys. Chem. B*, 2006, **110**, 21833-21839.

3. A. A. Peterson, F. Abild-Pedersen, F. Studt, J. Rossmeisl and J. K. Norskov, *Energy Environ. Sci.*, 2010, **3**, 1311-1315.
4. Y.-L. Lee, M. J. Gadre, Y. Shao-Horn and D. Morgan, *Phys. Chem. Chem. Phys.*, 2015, **17**, 21643-21663.
5. P. W. Atkins, in *Physical Chemistry*, 6th ed., Oxford University Press: Oxford, U. K., 1998, **485**, 925-927.
6. L. D. Chen, J. K. Nørskov and A. C. Luntz, *J. Phys. Chem. Lett.*, 2015, **6**, 175-179.
7. V. Viswanathan, H. A. Hansen, J. Rossmeisl and J. K. Nørskov, *J. Phys. Chem. Lett.*, 2012, **3**, 2948-2951.
8. J. Suntivich, H. A. Gasteiger, N. Yabuuchi and Y. Shao-Horn, *J. Electrochem. Soc.*, 2010, **157**, B1263.
9. R. D. Deegan, O. Bakajin, T. F. Dupont, G. Huber, S. R. Nagel and T. A. Witten, *Nature*, 1997, **389**, 827-829.
10. R. D. Deegan, O. Bakajin, T. F. Dupont, G. Huber, S. R. Nagel and T. A. Witten, *Phys. Rev. E*, 2000, **62**, 756-765.
11. Y. Garsany, O. A. Baturina, K. E. Swider-Lyons and S. S. Kocha, *Anal. Chem.*, 2010, **82**, 6321-6328.
12. Y. Liang, Y. Li, H. Wang, J. Zhou, J. Wang, T. Regier and H. Dai, *Nat. Mater.*, 2011, **10**, 780-786.
13. S. Wang, D. Yu, L. Dai, D. W. Chang and J.-B. Baek, *ACS Nano*, 2011, **5**, 6202-6209.
14. R. Zhou, Y. Zheng, M. Jaroniec and S.-Z. Qiao, *ACS Catal.*, 2016, **6**, 4720-4728.
15. W. Xiao, D. Wang and X. W. Lou, *J. Phys. Chem. C.*, 2010, **114**, 1694-1700.
16. Y. Meng, W. Song, H. Huang, Z. Ren, S.-Y. Chen and S. L. Suib, *J. Am. Chem. Soc.*, 2014, **136**, 11452-11464.
17. Y. Gorlin and T. F. Jaramillo, *J. Am. Chem. Soc.*, 2010, **132**, 13612-13614.
18. J. Duan, S. Chen, S. Dai and S. Z. Qiao, *Adv. Funct. Mater.*, 2014, **24**, 2072-2078.
19. Y. Gorlin, C.-J. Chung, D. Nordlund, B. M. Clemens and T. F. Jaramillo, *ACS Catalysis*, 2012, **2**, 2687-2694.